Journal of the Indian Institute of Science
A Multidisciplinary Reviews Journal
ISSN: 0970-4140 Coden-JIISAD

REVIEWS

Lamb Wave Propagation in Laminated Composite Structures

S. Gopalakrishnan

Abstract | Damage detection using guided Lamb waves is an important tool in Structural health Monitoring. In this paper, we outline a method of obtaining Lamb wave modes in composite structures using two dimensional Spectral Finite Elements. Using this approach, Lamb wave dispersion curves are obtained for laminated composite structures with different fibre orientation. These propagating Lamb wave modes are pictorially captured using tone burst signal.

Keywords: *Wave propagation, Lamb waves, Composites, Spectral Finite Elements, Symmetric and Antisymmetric modes.*

1 Introduction

In the recent years, there has been an increased use of composites, especially in aerospace vehicles due to its high strength-to weight and stiffness-to-weight ratio.[1] Unlike metals, composites exhibit many different failure modes such as delamination, fibre breaks, matrix cracks, debonds etc. In addition, composites are susceptible to host of manufacturing environmental induced defects such as porosity, moisture absorption etc.[2] These problems associated with composites demands that these structures be regularly inspected. Moreover, the design philosophy of composites are markedly different when compared metals. Most composites are today designed based on safe life design philosophy wherein the structures are designed with increased factor of safety. This will make the structures heavier and bulky thereby defeating the very purpose of using composites, which is to make lighter and structurally efficient structures. Hence, more and more designers are now moving towards damage tolerant design philosophy, wherein the design margins are drastically reduced with the condition that the structures designed with such philosophy are periodically inspected. The periodic inspection of structures using Non Destructive Evaluation (NDE) methods is termed as Structural Health Monitoring (SHM).

There are many NDE methods such as eddy currents, ultrasonics, computer tomography, computer thermography etc[3] that are traditionally used for structural inspections. Most of these are passive or sensor only methods and its applications in aerospace inspections are highly time consuming having very high life-cycle cost, poor damage detection sensitivity and they also require that the structures be out of service. Most of the SHM systems are active or sensor and actuator systems which act both as sensors and trigger systems. Many active SHM systems are based on a number of different sensors such as piezoelectric sensors (both ceramic and crystal forms) fibre optic sensors, magnetostrictive sensors such as TERFENOL-D, MEMS sensors are quite well developed. Reference[4] gives a good overview of these developments. Many of these SHM systems works in the principle of wave propagation, wherein an incident wave interacts with a damage and produces a unique signature that will help in identifying the location of the flaw (crack) using the wave dispersion and time of arrival of reflection information. Among the wave propagation based technique, the method based on Lamb wave is extensively used in SHM because of its ability to traverse large distances with very little attenuation. These are generated in a doubly bounded isotropic thin solid that have stress free boundary at the top and bottom surfaces as shown in Fig. 1.

In the Fig. 1, z is the thickness direction, where the total thickness of the plate is shown as $2h$. SHM process involves in triggering an incident wave in a structure that has stress free boundary at the top and bottom surfaces. There are two categories of Lamb waves; symmetric and antisymmetric

Department of Aerospace Engineering, Indian Institute of Science, Bangalore 560 012, India.
krishnan@aero.iisc.ernet.in

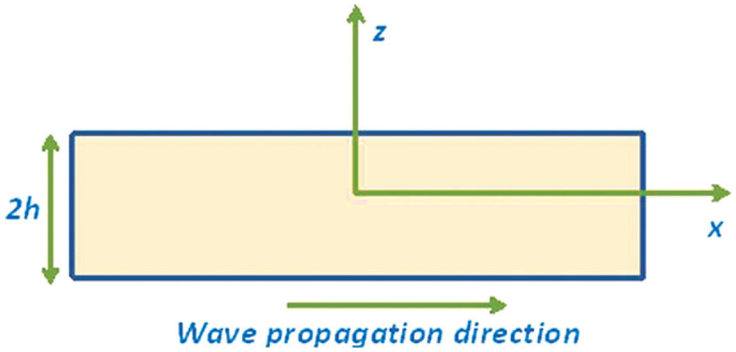

Figure 1: Coordinates for Lamb wave propagation.

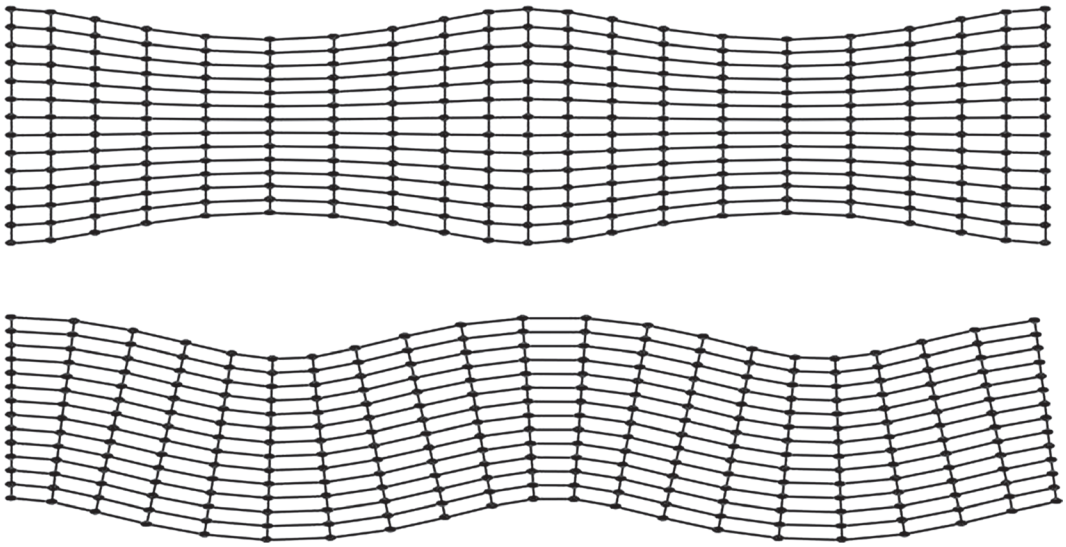

Figure 2: Lowest symmetric and antisymmetric Lamb wave modes in an isotropic waveguide.

depending upon the nature of propagation and type of propagation medium. There are many propagating Lamb waves in structures that are either symmetric or antisymmetric and the speeds of each of these wave modes depends on the frequency and hence these wave modes are highly dispersive in nature. The lowest of them are called the A_0 or S_0 depending upon the nature of waves and these are shown in Fig. 2.

Lamb wave modes were first obtained by Lamb,[5] for isotropic doubly bounded media by considering one of the dimensions of solid as infinite. Lamb wave modes can be obtained by solving the governing partial differential of a 2-D solid for a stress free boundary at the top and bottom surfaces. However the solution of the governing coupled partial differential equation is not trivial. For an isotropic structure, the governing equation is transformed into two independent partial differential equation, using Helmholtz decomposition. These partial differential equations have scalar and vector potentials as independent variable. These uncoupled equation are solved to obtain the Lamb wave modes. References,[6–8] give a good account of Lamb waves along with theoretical/analytical procedure to determine its dispersion relations in isotropic waveguides.

Understanding wave propagation is an order more complex compared to isotropic structures. Here, the wave propagation and its interactions depend on composite material properties, its ply orientation, its geometry, frequency, direction of propagation, and interfacial conditions. If the wavelengths are significantly longer than the smallest dimension in composites, namely the fibre diameter and their spacing, then each lamina can be considered as an equivalent homogenous that is orthotropic with axis of symmetry coinciding with the fibre orientation. Reference[9] performed experiments on boron/epoxy laminated

composites to study its dispersion and found that, for extensional waves, scattering began to show when the wavelength is of the same order of magnitude as the diameter of the fibre, while the flexural wave started to scatter when the ratio of wavelength to fibre diameter is about 40. In addition, composites are characterized by different interface conditions due to different properties across the laminae. Due to this, in addition to reflections from the interfaces, there will be refractions between layers that manifests in the form of resulting waves propagating along the plane of the plate. The direction of wave propagation dictates the velocity of wave and the material anisotropy makes the pure wave modes loose its properties. The dependence of wave velocity on the direction of propagation implies that the direction of group velocity does not generally coincide with the wave vector. Also, for a generally unsymmetric laminate, the material anisotropy makes the distinction between symmetric and antisymmetric modes very difficult and they are generally coupled. In design of composites, symmetric laminate is normally preferred and in such laminates, the symmetric and antisymmetric Lamb wave modes are uncoupled and they are normally termed as *quasi* symmetric or antisymmetric Lamb wave modes. Due to the above reasons, one cannot use Helmholtz decomposition (as was used for isotropic waveguides) to uncouple the governing 2-D equation of motion in terms of scalar and vector potentials.

Attempts have been made to obtain Lamb wave modes in composites both by exact solution of 3-D elasticity equations and through numerical solutions. Researchers[10–13] have attempted to solve 3-D elasticity equations to obtain Lamb wave modes in different composites waveguides. Although exact solutions provide accurate estimation of Lamb wave dispersion, their computations is computationally very intensive because, their solution involve solving highly nonlinear transcendental equations. Hence, many researchers have tried to use numerical solutions to determine the Lamb wave modes. In this direction, References[14–17] can be mentioned, who have attempted to solve the 3-D equations of motion numerically to obtain the Lamb wave modes.

In this paper, we will solve the governing equation through Spectral Finite Element Method (SFEM). Spectral finite element method is a finite element method that is formulated in the frequency domain. Fast Fourier Transform (FFT), which basically an implementation of Discrete Fourier Transform (DFT) is used to transform any time dependent variable back and forth between time and frequency domain. Unlike conventional finite element, SFEM requires strong form of the governing equation in the frequency domain, whose solution will be used as interpolating function for spectral finite element formulation. Dynamic stiffness matrix (which is single matrix, as opposed to conventional FEM, where two matrices, namely the stiffness and mass matrix will be required) is generated using the same procedure normally adopted to generate finite element matrices. Over a big frequency *do-loop*, the dynamic stiffness is generated, assembled and solved for a unit impulse, to obtain the Frequency Response Function, which is convolved with the load to obtain the frequency domain output. The time history of the output is then obtain by taking inverse FFT. Since exact solution to the governing equation is used as the basis function, one element is sufficient between any two joints. This is because the inertia distribution is exactly represented and as a result, the small wavelengths at high frequencies are very well captured. Hence SFEM problem sizes are many orders smaller than conventional finite elements. However SFEM can only be applied to linear problem due to the restriction of FFT and it can handle only simple domains where the wave equation can be solved exactly. Details of this method are given in.[6,7]

The procedure described above is valid only for 1-D wave equations, where the transformation of the governing partial differential equation to frequency domain will result in a set of ordinary differential equations with constant coefficients, whose solutions are well known. In 2-D wave equation, which is normally of Posson's type, transformation of the time variable to frequency domain does not result in ordinary differential equations. One more transform in one of the space variable is required to transform the governing partial differential equation to ordinary differential equations. This puts the restriction that one of the spatial domain is unbounded with an additional wavenumber introduced in the coordinate direction where the transform was taken. In this paper, we will use such a model to construct a 2-D spectral element for both in-plane and out-of plane loads and use the dynamic stiffness matrix of these elements to generate the Lamb wave dispersion plots for laminated composite structures.

The Spectral finite elements for isotropic 2-D waveguides were developed using the method of potentials, which is however applicable only for isotropic waveguides. Reference[18] gives a detailed outline of the 2-D spectral element for isotropic solids. For anisotropic media such as composites,

among the available methodologies, Partial Wave Technique (PWT) is an attractive option. In this paper, spectral finite elements are formed using the PWT, where we use the Singular Value Decomposition (SVD) method (please see[6] for more details) to obtain the wave amplitudes, which is essential for constructing the partial waves. Once the partial waves are found, the wave coefficients are made to satisfy prescribed boundary conditions, i.e., two non-zero tractions specified at the top and bottom of the layer. Here, it differs from other formulations based on the PWT, as no specific problem oriented boundary conditions are imposed. Thus a system matrix is established, which relates the tractions at the interface to the interfacial displacements. This generalization enables the use of the system matrix as a finite element dynamic stiffness matrix, although formulated in frequency/wavenumber domain. These matrices can be assembled to model different layer of different ply-orientation or inhomogeneity, which obviates the necessity of cumbersome computation associated with multilayer analysis, (e.g.,[19]).

This paper is organized as follows: First the derivation of Lamb waves in metallic structures is presented. Although its derivation is available in classic text books,[7,19] the aim here is to two fold; one is to see how the Lamb wave modes in metal differ from composites and the second is to see how the present approach of determination of Lamb wave modes using PWT is different from the method of potentials normally used for metallic waveguides. Next, spectral element formulation for layered composites is presented. This is followed by a presentation on the detailed procedure to compute Lamb wave modes using the formulated spectral elements. Finally, some numerical examples are provided for determination of Lamb wave modes and their time responses as function of ply orientation.

2 Lamb Waves in Doubly Bounded Metallic Waveguides

To derive the Lamb wave modes in metallic structure, we will have to start from the governing differential equation, which in terms of stress tensor σ_{ij} and body force b_i is given in tensorial notation

$$\frac{\partial \sigma_{ij}}{\partial x_j} + b_i = \rho \ddot{u}_i \tag{1}$$

where, $x_i = x_2, x_3$ with $x_1 = x$, $x_2 = y$, $x_3 = z$ are the three coordinate directions and ρ is the density and $\ddot{u}_i$ are the component of acceleration in the three coordinate directions. The relation between the strains, rotations and displacements are given by

$$\in_{ij} = \frac{1}{2}\left(\frac{\partial u_i}{\partial x_j} + \frac{\partial u_j}{\partial x_i}\right), \quad \omega_{ij} = \frac{1}{2}\left(\frac{\partial u_i}{\partial x_j} + \frac{\partial u_j}{\partial x_i}\right) \tag{2}$$

Most metallic structures are assumed isotropic and the Hook's law for isotropic structures in tensor notation is given by

$$\sigma_{ij} = 2\mu \in_{ij} + \lambda \in_{kk} \delta \tag{3}$$

where μ and λ are the Lame' constants and δ_{ij} is the Kronecker delta. Using the strain displacement relationship and the Hook's law, one can express stresses in terms of displacement, which can be substituted in Eqn. (1), to get the governing equation in terms of displacement and this equation is called the *Navier's Equation*, which can be expressed in tensorial notation as

$$(\lambda + \mu) u_{k,ki} + \mu u_{i,kk} + b_i = \rho \ddot{u}_i \tag{4}$$

Equation (4) represents three highly coupled partial differential equations in terms of displacements, which are extremely difficult to solve. Hence, we use the method potentials or Helmholtz decomposition to solve the above equation. The Helmholtz decomposition enables the displacement of the isotropic solid to be expressed in terms of a scalar potential Φ and the vector potential $H_i = H_1, H_2, H_3$ as

$$u_i = \frac{\partial \Phi}{\partial x_i} + \in_{ipq} \frac{H_q}{\partial x_p}, \quad \frac{\partial H_k}{\partial x_k} = 0 \tag{5}$$

where $\in_{ipq}$ is the permutation symbol. Equation (5) represents three displacements $u_1 = u$, $u_2 = v$, $u_3 = w$ with four potentials Φ, H_1, H_2 and H_3. Note that the second condition in Eqn. (5) uniquely determines the vector potential H_i. On substituting Eqn. (5) in Eqn. (4), we get after rearranging

$$\frac{\partial}{\partial x_i}\left[c_p^2 \nabla^2 \Phi - \ddot{\Phi}\right] + \frac{\partial}{\partial x_p}\left[c_s^2 \nabla^2 H_q - \ddot{H}_q\right] \in_{pqi} = 0 \tag{6}$$

where the Laplacian is given by

$$\nabla^2 = \frac{\partial^2}{\partial x^2} + \frac{\partial^2}{\partial y^2} + \frac{\partial^2}{\partial z^2} \tag{7}$$

These equations are satisfied if the terms inside the square brackets are zero. That is if Φ and H_q are chosen such that

$$c_p^2 \nabla^2\Phi - \ddot{\Phi} = 0, \qquad c_s^2 \nabla^2 H_q - \ddot{H}_q = 0 \tag{8}$$

where c_p is called the *P-wave* or *dilatational* or *Longitudinal* wave speeds and c_s is called the *S-wave* or *distortional* or *Shear* wave speed and they are given by

$$\begin{aligned} c_p^2 &= \frac{\lambda+2\mu}{\rho} = \frac{E(1-\nu)}{\rho(1+\nu)(1-2\nu)}, \\ c_s^2 &= \frac{\mu}{\rho} = \frac{G}{\rho} = \frac{E}{2\rho(1+\nu)} \end{aligned} \tag{9}$$

Solution of Eqns. (8) are lot simpler compared to the original highly coupled partial differential equation Eqn. (4).

The solution of Eqn. (8) is of the following form

$$\begin{aligned} \Phi(x,y,z,t) &= Y_P(y)e^{-i(kx-\omega t)}, \\ H_z(x,y,z,t) &= Y_S(y)e^{-i(kx-\omega t)} \end{aligned} \tag{10}$$

where the *x, y, z* are the coordinate directions shown in Fig. 1. In the above equation, the solution of $Y_p(y)$ and $Y_S(y)$ are different for symmetric and antisymmetric modes and they take the following form:

(a) Symmetric Modes:

$$Y_P(y) = A\cos(\eta y), \qquad Y_s(y) = B\sin(\bar{\eta} y) \tag{11}$$

(b) Antisymmetric Modes:

$$Y_P(y) = C\sin(\eta y), \qquad Y_s(y) = D\cos(\bar{\eta} y) \tag{12}$$

where the constants *A*, *B*, *C* and *D* needs to be determined through stress free boundary conditions, which needs to be imposed. We will now outline the procedure for symmetric modes. Knowing the potentials, we can write the displacement fields from Eqn. (5), which for 2-D case becomes

$$u(x,y,t) = \frac{\nabla\Phi}{\partial x} + \frac{\partial H_z}{\partial y}, \quad v(x,y,t) = \frac{\partial\Phi}{\partial y} + \frac{\partial H_z}{\partial x} \tag{13}$$

Substituting the value of potentials from Eqn. (10), the displacements can be rewritten as

$$u = \left[\, ikA\cos(\eta y) + \bar{\eta}\cos(\eta y)\right] e^{-i(kx-\omega t)} \tag{14}$$

$$v = \left[\, -i\eta A\sin(\eta y) + ikB\cos(\bar{\eta} y\right] e^{-i(kx-\omega t)} \tag{15}$$

It is apparent that the specific choice of Y_p and Y_S gives displacements in *x* direction that are symmetric with respect to *y* direction. Next, we will evaluate strains using the strain displacement relations given by Eqn. (2). This is then used in the hooks law given by Eqn. (3), which can be simplified as

$$\begin{aligned} \sigma_{xx} = \Big[&-\left(2\mu k^2 + k_p^2\right) A\cos(\eta y) \\ &-2\mu(ik\bar{\eta})B\cos(\bar{\eta} y)\Big] e^{-i(kx-\omega t)} \end{aligned} \tag{16}$$

$$\begin{aligned} \sigma_{yy} = \Big[&\mu(k^2 - \eta^2)A\cos(\eta y) \\ &+ 2\mu(ik\bar{\eta})B\cos(\bar{\eta} y)\Big] e^{-i(kx-\omega t)} \end{aligned} \tag{17}$$

$$\begin{aligned} \sigma_{xy} = \Big[&\mu(2ik\eta)A\sin(\eta y) \\ &-\mu(\bar{\eta}^2 - k^2)B\sin(\bar{\eta} y)\Big] e^{-i(kx-\xi t)} \end{aligned} \tag{18}$$

Now we will enforce stress free conditions at the boundary $y = \pm h$, that is, at $y = \pm h$, we have $\sigma_{yy} = 0$ and $\sigma_{xy} = 0$ is enforced. In doing so, we get following matrix equation

$$\begin{bmatrix} (k^2 - \eta^2)\cos(\eta h) & 2ik\bar{\eta}\cos(\bar{\eta} h) \\ 2ik\eta\sin(\eta h) & (k^2 - \bar{\eta}^2)\sin(\bar{\eta} h) \end{bmatrix} \begin{Bmatrix} A \\ B \end{Bmatrix} = 0 \tag{19}$$

Setting the determinant of above matrix to zero will get us the following transcendental equation for solution of horizontal wavenumbers η and $\bar{\eta}$

$$\frac{\tan(\eta h)}{\tan(\bar{\eta} h)} = -\frac{4k^2\eta\bar{\eta}}{(\bar{\eta}^2 - k^2)^2} \tag{20}$$

Following the same procedure and starting with Eqn. (12), we can get the following transcendental equation for obtaining antisymmetric modes

$$\frac{\tan(\bar{\eta} h)}{\tan(\eta h)} = -\frac{4k^2\eta\bar{\eta}}{(\bar{\eta}^2 - k^2)^2} \tag{21}$$

In the above equations, η and $\bar{\eta}$ are given by

$$\eta = \sqrt{\left(\frac{\omega}{c_p}\right)^2 - k^2}, \qquad \bar{\eta} = \sqrt{\left(\frac{\omega}{c_s}\right)^2 - k^2} \tag{22}$$

where c_p and c_s are given by Eqn. (9).

Solution of Eqns. (20) and (21) is not trivial and requires numerical methods to solve in order to determine the Lamb wave modes. We see that for

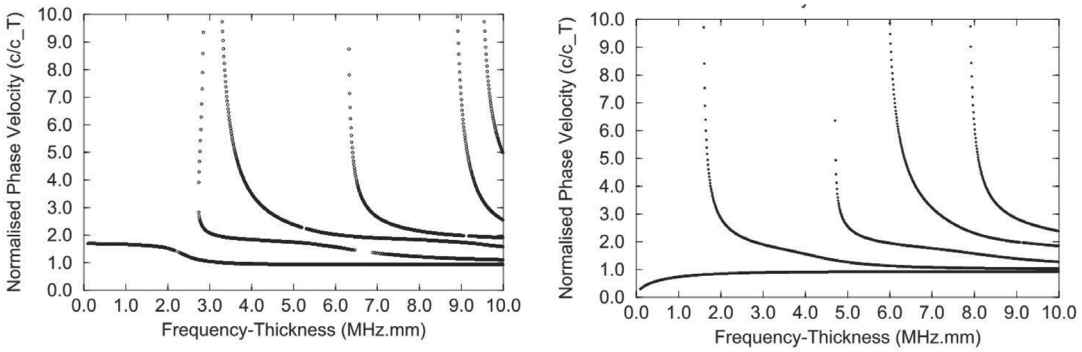

(a) Symmetric Lamb wave modes (b) Antisymmetric Lamb wave modes

Figure 3: Dispersion curves for symmetric and antisymmetric Lamb wave modes in Aluminium.

a given value of ω, Eqns. (20) and (21) specifies the value of wavenumbers η and $\bar{\eta}$ that the waves can allow and hence the speeds of these waves. These wavenumbers have nonlinear relationship with frequency ω indicating that the waves are dispersive. In addition, Eqns. (20) and (21) are in terms of product ωh, normally called *frequency-thickness* product and hence it is traditional to plot the wave speeds of the Lamb waves as a function of *frequency-thickness* product. Also, if we look at these equations, we see that the relationship between η and $\bar{\eta}$ and hence the wavenumber k and the frequency ω is obviously multivalued and these needs to be obtained numerically. Each of these values obtained is called a *mode* and the lowest symmetric mode is called the S_0 mode, while the lowest antisymmetric mode is called the A_0 mode. As ωh increases, new wave modes appear and these are labelled as S_n and A_n modes according to the order in which they appear. Using a Newton-Rhapson technique, Eqns. (20) and (21) were solved and the phase speeds, which is equal to ω/k and the group speeds, which is equal to $d\omega/dk$ are extracted. The phase speed plot is shown in Fig. 3.

3 Spectral Element Formulation for Laminated Composites

The general elasto-dynamic equation of motion for three dimensions is given by

$$\sigma_{ij,j} = \rho \ddot{u}_i, \quad \sigma_{ij} = C_{ijkl} \in_{kl}, \quad \in_{ij} = (u_{i,j} + u_{j,i})/2 \tag{23}$$

where comma (,) and dot over a variable denote partial differentiation with respect to the spatial variables and time, respectively. For 2-D model with orthotropic material construction, complexity of the above equation can be further reduced by the following assumptions. The non-zero displacements are $u_1 = u$ and $u_3 = w$ in the direction $x_1 = x$ and $x_3 = z$, respectively (see Fig. 4). Then the non-zero strains are related to these displacements by

$$\in_{xx} = u_x, \quad \in_{zz} = w_z, \quad \in_{xz} = u_z + w_x \tag{24}$$

The nonzero stresses are then related to the strains by the relation

$$\begin{aligned} \sigma_{xx} &= Q_{11} \in_{xx} + Q_{13} \in_{zz}, \\ \sigma_{zz} &= Q_{13} \in_{xx} + Q_{33} \in_{zz}, \\ \sigma_{xz} &= Q_{55} \in_{xz} \end{aligned} \tag{25}$$

where Q_{ij}s are the stiffness coefficients, which depend on the ply layup, its orientation and z coordinate of the layer. The expressions of the Q_{ij}s are given in.[20] Substituting Eqn. (25) in Eqn. (23) and imposing the assumptions, the elastodynamic equation for 2-D inhomogeneous orthotropic media is given by

$$\begin{aligned} Q_{11} u_{xx} + (Q_{13} + Q_{55}) w_{xz} + Q_{55} u_{zz} &= \rho \ddot{u}, \\ Q_{55} w_{xx} + (Q_{13} + Q_{55}) u_{xz} + Q_{33} w_{zz} &= \rho \ddot{w} \end{aligned} \tag{26}$$

The displacement field is assumed to be a synthesis of frequency and wavenumbers, both horizontal and vertical, as

$$u(x,z,t) = \sum_{n=1}^{N-1} \sum_{m=1}^{M-1} \hat{u}_{nm}(z, \eta_m, \omega_n) \begin{Bmatrix} \sin(\eta_m x) \\ \cos(\eta_m x) \end{Bmatrix} e^{-j\omega_n t} \tag{27}$$

$$w(x,z,t) = \sum_{n=1}^{N-1} \sum_{m=1}^{M-1} \hat{w}_{nm}(z, \eta_m, \omega_n) \begin{Bmatrix} \cos(\eta_m x) \\ \sin(\eta_m x) \end{Bmatrix} e^{-j\omega_n t} \tag{28}$$

where ω_n is the discrete angular frequency, η_m is the discrete horizontal wavenumber and $j^2 = -1$. As the assumed field suggests, for $M \to \infty$, the model will

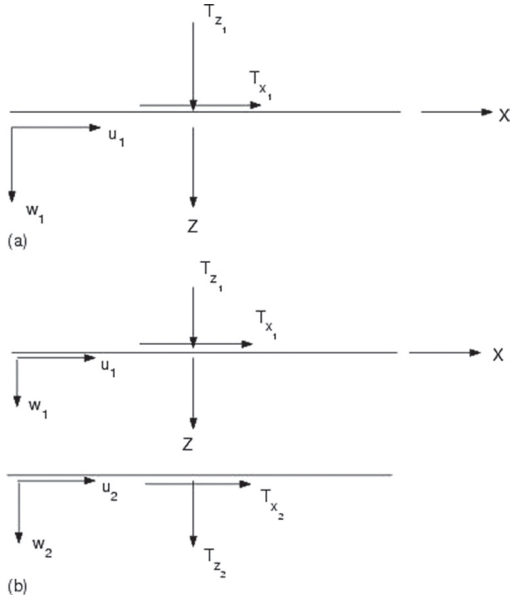

Figure 4: Spectral layer element: Sign conventions of (a) throw-off spectral element (b) finite composite layer element.

have infinite extent in positive and negative X direction, although of finite extent in the Z direction, i.e., it will be a layered structure. In particular, the domain can be written as $\Omega = [-\infty, +\infty] \times [0, L]$ where L is the thickness of the layer. The boundaries of any layer will be specified by a fixed value of z. The X dependency of the displacement field (sine or cosine) will be determined based upon the loading pattern. In all subsequent formulation and computation, symmetric load pattern will be considered. The real computational domain is where X_L is the X window length. Discrete values of η_m depend upon the X_L and the number of mode shapes (M) chosen.

Assuming the displacement filed as given in Eqns. (27) and (28), the governing PDE is reduced to

$$[A]\hat{u}'' + [B]\hat{u}' + [C]\hat{u} = 0, \quad \hat{u} = \{\hat{u}\ \hat{w}\} \tag{29}$$

where prime denotes differentiation with respect to z. The matrices [**A**], [**B**] and [**C**] are

$$[A] = \begin{bmatrix} Q_{55} & 0 \\ 0 & Q_{33} \end{bmatrix},$$
$$[B] = \begin{bmatrix} 0 & -(Q_{13}+Q_{55})\eta_m \\ (Q_{13}+Q_{55})\eta_m & 0 \end{bmatrix}, \tag{30}$$
$$[C] = \begin{bmatrix} -\eta_m^2 Q_{11} + \rho\omega_n^2 & 0 \\ 0 & -\eta_m^2 Q_{55} + \rho\omega_n^2 \end{bmatrix}$$

The solution to these ODEs are of the form $u_o e^{-jkz}$ and $w_o e^{-jkz}$, which yields the Polynomial Eigenvalue Problem (PEP) (for details of PEP please refer to[6])

$$\begin{aligned} &[W]\{u_o\} = 0, \\ &[W] = -k^2[A] - jk[B] + [C], \\ &\{u_o\} = \{u_o\ w_o\} \end{aligned} \tag{31}$$

where ***W***, the wave matrix is

$$[W] = \begin{bmatrix} -k^2 Q_{55} - \eta_m^2 Q_{11} + \rho\omega_n^2 & jk\eta_m(Q_{13}+Q_{55}) \\ -jk\eta_m(Q_{13}+Q_{55}) & -k^2 Q_{33} - \eta_m^2 Q_{55} + \rho\omega_n^2 \end{bmatrix} \tag{32}$$

The singularity condition of $[W]$ yields

$$\begin{aligned} &Q_{33}Q_{55}k^4 + \left\{(Q_{11}Q_{33} - 2Q_{13}Q_{55} - A_{13}^2)\eta_m^2 \right. \\ &\left. - \rho\omega_n^2(Q_{33}+Q_{55})\right\}k^2 + \left\{Q_{11}Q_{55}\eta_m^4 \right. \\ &\left. - \rho\omega_n^2\eta_m^2(Q_{11}+Q_{55}) + \rho^2\omega_n^4\right\} = 0 \end{aligned} \tag{33}$$

The above equation which relates vertical wavenumber k to the horizontal wavenumber η frequency ω is the spectrum relation. It is to be noted that for each value of η_m and ω_n, there are four values of k, denoted by k_{lmn}, $l = 1.4$, which is obtained by solving the spectrum relation. Explicit solution of the wavenumber k is $k_{lmn} = \pm\sqrt{-b \pm \sqrt{b^2 - 4ac}}$, where a, b and c are the coefficients of k^4, k^2 and k^0, respectively, in Eqn. (33).

There are certain properties of the wavenumbers which will be explored now. As can be seen from Eqn. (33), for $\eta_m = 0$, the equation is readily solvable to give the roots $\pm\omega\sqrt{\rho/Q_{33}}$ and $\pm\omega\sqrt{\rho/Q_{55}}$. Since, none of the ρ, Q_{33} or Q_{55} can be negative or zero, these roots are always real and linear with ω. When η_m is not zero, k becomes zero for ω satisfying

$$\begin{aligned} &Q_{11}Q_{55}\eta_m^4 - \rho\omega_n^2\eta_m^2(Q_{11}+Q_{55}) + \rho^2\omega_n^4 = 0 \quad \text{or} \\ &(Q_{11}\eta_m^2 - \rho\omega^2)(Q_{55}\eta_m^2 - \rho\omega^2) = 0 \end{aligned} \tag{34}$$

which gives

$$\omega = \eta_m\sqrt{Q_{11}/\rho}, \quad \eta_m\sqrt{Q_{55}/\rho} \tag{35}$$

Before these frequencies, the roots are imaginary and non-propagating and after these frequencies, the roots are real and propagating. These frequencies are the cut-off frequencies. For isotropic materials they are given by $C_p\eta$ and $c_s\eta$.[18] The current expressions

for the cut-off frequencies are also reducible to that of isotropic materials if we identify Q_{11} and Q_{55} with $\lambda + 2\mu$ and μ, respectively, where λ and μ are the Lame's parameters. If we identify *QP* wave with Q_{33} (or Q_{11}) and *QSV* wave with Q_{55}, then as the cut-off frequencies suggest, for the same value of η, it is the *QSV* wave that becomes propagating first, since $Q_{11} > Q_{55}$. The wavenumbers of positive roots denote forward propagating modes and the negative roots denote backward propagating modes. In Fig. 5, the wavenumbers are plotted for three different ply-angles, 0°, 45°, and 90°. For all the ply-angles, Q_{33} and Q_{55} are assumed 9.69 GPa and 4.13 GPa, respectively. For Q_{11} and Q_{13}, following values are assumed. For 0°, Q_{11} = 146.3 GPa and Q_{13} = 2.98 GPa, for 45°, Q_{11} = 44.62 GPa and Q_{13} = 1.62 GPa and for 90°, Q_{11} = 9.69 GPa and Q_{13} = 2.54 GPa. In Fig. 5, imaginary part of the wavenumbers is plotted in horizontal plane and real part in the vertical plane. Further, the imaginary part of the wavenumbers for 0° and 90° are plotted in the positive side, whereas for 45° it is plotted in the negative side, for distinction. Two different η values are taken. The linear variation of the real part of the wavenumbers is for $\eta = 0$ and rest of the plots are for $\eta = 10$. The slope of the linear portion depends upon Q_{33} and Q_{55} and as they are equal for all the ply-angles, this part is common for all the ply-angles. The difference comes in the imaginary part and cut-off frequencies. Two different cut-off frequencies are seen in the figure for each ply-angle, where the largest value is for 0° ply-angle because of its largest Q_{11}. Further, the shear cut-off frequency is same for all the ply-angles as Q_{55} is equal in all the cases.

Once, the required wavenumbers k are obtained, for which the wave matrix [**W**] is singular, the solution u_0 for frequency ω_n and wavenumber η_m is

$$\hat{u}_{nm} = R_{11}C_1e^{-jk_1x} + R_{12}C_2e^{-jk_2x} + R_{13}C_3e^{-jk_3x} + R_{14}C_4e^{-jk_4x} \quad (36)$$

$$\hat{w}_{nm} = R_{21}C_1e^{-jk_1x} + R_{22}C_xe^{-jk_2x} + R_{23}C_3e^{-jk_3x} + R_{24}C_4e^{-jk_4x} \quad (37)$$

where R_{ij} are the amplitude coefficients to be determined and they are called wave amplitudes, which are determined using the method of SVD (Please see[6] for more details). R_{ij} are obtained from the wave matrix [**W**] evaluated at wavenumber k_i.

Once the four wavenumbers and wave amplitudes are known, the four partial waves can be constructed and the displacement field can be written as a linear combination of the partial waves. Each partial wave is given by

$$a_i = \begin{Bmatrix} u_i \\ w_i \end{Bmatrix} = \begin{Bmatrix} R_{1i} \\ R_{2i} \end{Bmatrix} e^{-jk_iz} \begin{Bmatrix} \sin(\eta_m x) \\ \cos(\eta_m x) \end{Bmatrix} e^{-j\omega_n t}, i = 1...4 \quad (38)$$

and the total solution is

$$u = \sum_{i=1}^{4} C_i a_i \quad (39)$$

Now, two different spectral element, one that is doubly bounded, which we call as *Finite Layer Composite Element* and the second, which is singly bounded media, which we call as *Infinite Layer Composite Element*. These are shown in Fig. 4. Unlike conventional finite elements, these elements are edge elements, that is the entire surface is designated as nodes. Each ply of the laminated composite is considered as an element in this approach. Infinite layer elements are those which

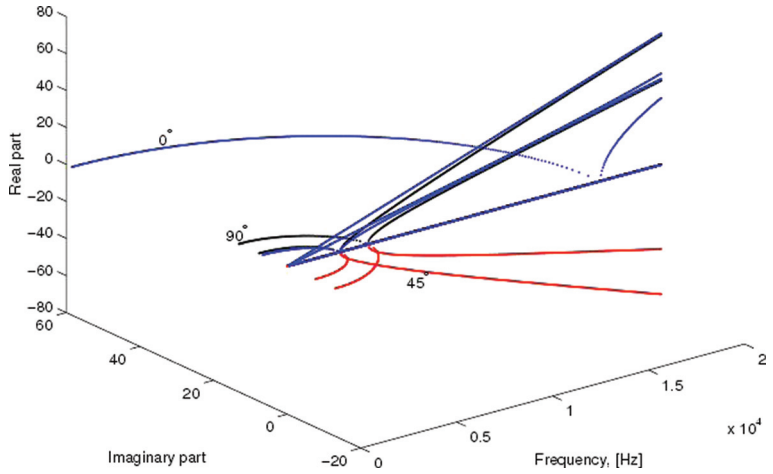

Figure 5: Variation of wavenumber with ω_n (for η_m = 10).

are non resonant, that is, the incident waves does not get reflected as the boundary rests at infinity.

3.1 *Finite layer composite element*

Once the solutions of u and w are obtained in the form of Eqns. (36) and (37) for each value of ω_n and η_m, we need to determine the dynamic stiffness matrix, that related the frequency domain displacements and the surface tractions. Thus, nodal displacements are related to the unknown constants by

$$\{\hat{u}_{1nm}\ \hat{w}_{1nm}\ \hat{u}_{2nm}\}^T = [T_1]_{nm}\{C_1\ C_2\ C_3\ C_4\}^T \tag{40}$$

That is,

$$\{\hat{u}\}_{nm} = [T_1]_{nm}\{C\}_{nm} \tag{41}$$

Using Eqn (25), nodal tractions are related to the constants by

$$\{\hat{t}\}_{nm} = [T_2]_{nm}\{C\}_{nm}, \{\hat{t}\}_{nm} = \{\sigma_{zz1}\ \sigma_{xz1}\ \sigma_{zz2}\ \sigma_{xz2}\}^T \tag{42}$$

Explicit forms of $[T_1]_{nm}$ and $[T_2]_{nm}$ are

$$[T_1] = \begin{bmatrix} R_{11} & R_{12} & R_{13} & R_{14} \\ R_{21} & R_{22} & R_{23} & R_{24} \\ R_{11}e^{(-jk_1L)} & R_{12}e^{(-jk_{21}L)} & R_{13}e^{(-jk_1L)} & R_{14}e^{(-jk_2L)} \\ R_{21}e^{(-jk_1L)} & R_{22}e^{(-jk_{21}L)} & R_{23}e^{(-jk_1L)} & R_{24}e^{(-jk_2L)} \end{bmatrix} \tag{43}$$

and

$$\begin{aligned} T_2(1,p) &= -Q_{55}(-jR_{1p}k_p - \eta R_{2p}) \\ T_2(2,p) &= jQ_{33}R_2k_p - Q_{13}\eta R_{1p} \\ T_2(3,p) &= Q_{55}(-jR_{1p}k_p - \eta R_{2p})e^{(-jk_pL)} \\ T_2(4,p) &= \{-jQ_{33}R_2k_p + Q_{13}\eta R_{1p}\}e^{(-jk_pL)} \end{aligned}$$

where p ranges from 1 to 4.

Thus, the dynamic stiffness matrix becomes

$$[\hat{K}]_{nm} = [T_2]_{nm}[T_1]^{-1}_{nm} \tag{44}$$

which is of size 4 × 4 and having ω_n and η_m as parameters. This matrix represents the dynamics of an entire layer of any length L at frequency ω_n and horizontal wavenumber η_m. Consequently, this small matrix acts as a substitute of the global stiffness matrix of FE modelling, whose size, depending upon the thickness of the layer, will be many orders larger than the formulated spectral finite element size.

3.2 *Infinite layer composite element*

This is the 2D counterpart of the 1D throw-off element (see[6] for details on the throw-off elements). The element is formulated by considering only the forward moving components, which means no reflection will come back from the boundary. This element acts as a conduit to throw away energy from the system and is very effective in modelling infinite domain in the Z direction. This element is also used to impose absorbing boundary conditions or to introduce maximum damping in the structure. The element has only one edge where displacements are to be measured and tractions are to be specified. The displacement field for this element (at ω_n and η_m) is

$$\hat{u}_{nm} = R_{11}C_{1nm}e^{-jk_1z} + R_{12}C_{2nm}e^{-jk_2z} \tag{45}$$

$$\hat{w}_{nm} = R_{21}C_{1nm}e^{-jk_1z} + R_{22}C_{2nm}e^{-jk_2z} \tag{46}$$

where it is assumed that k_1 and k_2 are having positive real parts. Following the same procedure as before, displacement at node 1 can be related to the constants C_i, $i = 1\ldots2$ as

$$\{\hat{u}\}_{nm} = [T_1]_{nm}\{C\}_{nm} \tag{47}$$

Similarly, tractions at node 1 can be related to the constants as

$$\{t_{x1}\ t_{y1}\}^T = [T_2]_{nm}\{C_{1nm}\ C_{2nm}\}^T, \quad \text{or} \quad \{\hat{t}\}_{nm} = [T_2]_{nm}\{C\}_{nm} \tag{48}$$

Explicit forms of the matrix $[\boldsymbol{T}_1]$ and $[\boldsymbol{T}_2]$ are

$$\begin{aligned} T_{1(ILE)} &= T_{1(FLE)}(1:2,1:2), \\ T_{2(ILE)} &= T_{2(FLE)}(1:2,1:2) \end{aligned} \tag{49}$$

The dynamic stiffness for the inhomogeneous infinite half space becomes

$$[\hat{K}]_{nm} = [T_2]_{nm}[T_1]^{-1}_{nm} \tag{50}$$

which is a 2 × 2 and the entries of this matrix are always complex.

4 Determination of Lamb Wave Modes

As mentioned earlier, Lamb waves are guided waves (see Fig. 1), propagating in a free plate and the two lateral guiding surfaces are traction free. There are two main approaches to the analysis of the Lamb waves. The first one is the method of potentials, which was explained in Section 2. In this method, Helmholtz decomposition of the displacement field is used and the governing equations are uncoupled and written in terms of the potentials. Solutions are sought for these potentials, which

contain four arbitrary constants. The displacement field and the stresses are expressed in terms of the potentials and the imposition of the tractions free upper and lower surfaces generates the necessary condition for finding the unknown constants and the dispersion equation. The advantage of this method is that the symmetric and anti-symmetric modes can be isolated during formulation, (see Fig. 2). However, the method is applicable only to the isotropic materials. This approach was presented in Section 2.

The second approach is based on Partial Wave Technique, which was used to derive the spectral finite element for laminated composites, and this is discussed below in detail. In the spectral finite element formulation, there are two summations in the solutions (see Eqns. (27) and (28)). The outer one is over discrete frequencies and the inner one is over discrete horizontal wavenumbers. Each partial wave of Eqn. (39) satisfies the governing PDEs (Eqn. 26) and the coefficients C_i as a whole satisfy any prescribed boundary conditions. As long as the prescribed natural boundary conditions are non-homogeneous, no restriction upon the horizontal wavenumber η_m is imposed and that leads to double summation solution of the displacement field. However, that is not the case for traction free boundary conditions on the two surfaces, which are the necessary condition for generating Lamb waves. The governing discrete equation for finite layer (Eqn. 44) in this case becomes

$$[\hat{K}(\eta_m,\omega_n)]_{nm}\{\hat{u}\}_{nm}=0 \tag{51}$$

and we are interested in a nontrivial $\{\boldsymbol{u}\}$. Hence, the stiffness matrix $[\hat{K}]$ must be singular, i.e., $det(\hat{K}(\eta_m,\omega_n))=0$, which is the required relation between ω_n and η_m. Since, ω_n is made to vary independently, above relation must be solved for η_m to render the stiffness matrix singular, i.e., η_m cannot vary independently. More precisely, for each value of ω_n there is a set of values of horizontal wavenumber η_m (one for each mode) and for each value of ω_n and η_m there are 4 vertical wavenumbers k_{nm}. Normally for the wave propagation response problem, will assume η as

$$\begin{aligned}&\omega_n=2n\pi/T=2n\pi/(N\Delta t),\\&\eta_m=2(m-1)\pi/X_L=2(m-1)\pi/(M\Delta x)\end{aligned} \tag{52}$$

where Δt and Δx are the temporal and spatial sample rate, respectively. The difference in this case is in the value of η_m, which is to be solved for, as opposed to its expression in Eqn. (52) and M is the number of Lamb modes considered rather than Fourier modes. Now, for each set of $(\omega_n, \eta_m, k_{nml})$, $l=1....4$, $\hat{K}$ will be singular and will be in the null space of $\hat{K}$. Now using Eqn.(39), total solution can be constructed. For prescribing traction free conditions at the top and bottom surfaces, we need to extract stresses from the displacements. From the displacement field (Eqns. (36) and (37), strain-displacement relation, Eqn. (24), stress-strain relation Eqn. (25), the matrix of strain-nodal displacement relation and stress-nodal displacement relation can be established as

$$\begin{aligned}&\{\in\}=[B][T_1]^{-1}\{\hat{u}\},\quad \{\sigma\}=[Q][B][T_1]^{-1}\{\hat{u}\},\\&\{\in\}=\{\in_{xx},\in_{zz},\in_{xz}\},\quad \{\sigma\}=\{\sigma_{xx},\sigma_{zz},\sigma_{xz}\}\end{aligned} \tag{53}$$

where the elements of $[\boldsymbol{B}]$(size 3×4) are described in terms of the wave amplitude matrix $[\boldsymbol{R}]$as

$$\begin{aligned}&B(1,p)=R_{1p}\eta e^{-jk_pz},\ B(2,\rho)=-jR_{2p}k_pe^{-jk_pz},\\&B(3,p)=-(jR_{1p}k_p+R_{2p}\eta)e^{-jk_pz},\quad p=1,...,4\end{aligned} \tag{54}$$

where z is the point of strain measurement. The elasticity matrix $[\boldsymbol{Q}]$ is

$$[Q]=\begin{bmatrix}Q_{11}&Q_{13}&0\\Q_{13}&Q_{33}&0\\0&0&Q_{55}\end{bmatrix} \tag{55}$$

Following the normal practice, the traction free boundary conditions (i.e., $\sigma_{zz}, \sigma_{xz}=0$) are prescribed at $z=\mp h/2$. Using Eqn. (53), the governing equation for C_i and η_m becomes

$$\begin{aligned}&[W_2(\eta_m,\omega_n)]\{C\}_{nm}=0,\\&\{C\}=\{C_1\quad C_2\quad C_3\quad C_4\}^T\end{aligned} \tag{56}$$

where $[\boldsymbol{W_2}]$ is another form of the stiffness matrix $[\boldsymbol{K}]$ and is given by

$$\begin{aligned}&W_2(1,p)=(Q_{11}R(1,p)\eta-jQ_{13}R(2,p)k_p)e^{j(k_p)h/2},\\&W_2(2,p)=(Q_{11}R(1,p)\eta-jQ_{13}R(2,p)k_p)e^{-j(k_p)h/2},\\&W_2(3,p)=Q_{55}(-R(1,p)k_p+jR(2,p)\eta)e^{j(k_p)h/2},\\&W_2(4,p)=Q_{55}(-R(1,p)k_p+jR(2,p)\eta)e^{-j(k_p)h/2}\end{aligned}$$

The dispersion relation is $det[\boldsymbol{W_2}]=\boldsymbol{0}$, which will yield $\eta_m(\omega_n)$ and the phase speed for Lamb waves c_{nm} will be given by ω_n/η_m. Once the values of η_m are known for the desired number of modes, the elements of $\{\boldsymbol{C}\}_{nm}$ are obtained by the technique of SVD as described earlier to find the elements of $[\boldsymbol{R}]$. Summing over all the Lamb modes, the solution for each frequency is obtained.

5 Lamb Wave Modes in Composite Waveguides

In this section, we present some dispersion curves for laminated composites structures for different ply orientations using the formulated spectral element. The developed model requires that every ply be considered as a spectral element, in other words, if there are n plies in a laminated composite structures, then such a structure will have to be modelled by n spectral elements.

An angle-ply lamina of 2 mm thickness is considered for the study of propagating Lamb wave modes. Analysis is performed for three different fibre-directions, 0°, 45°, and 90°. Material properties of the composite are as in Section 3 used for computing wavenumbers. The dispersion relation (relation between $C_p = \omega/\eta$ and ω) is obtained and plotted for each of the above ply orientation mentioned above. Apart from the choice of algorithm there are other subtle issues in root capturing for the solution of wavenumbers as the solutions are complicated in nature.

Moreover, except the first one or two modes, all the other roots escape to infinity at low frequency. For isotropic materials, these cut-off frequencies are known below which the phase speeds are infinite. However, no expressions can be found for composite waveguides and most of the times, the modes (solutions) should be tracked backward, i.e., from higher frequency to lower frequency. In general two strategies are essential to capture all the modes within a given frequency band. Initially, the whole region should be swept for different values of the initial guess, where the initial guess should remain constant for the whole range of frequency. These sweeping opens up all the modes in that region, although they are not completely traced. Subsequently, each individual mode should be followed to the end of the domain or to a pre-set high value of the solution. For this case, the initial guess should be changed for each frequency to the solution of the previous frequency step. Also, sometimes it is necessary to reduce the frequency step in the vicinity of high gradient of the modes. Once the Lamb modes are generated, they are fed back into the frequency loop to generate the frequency domain solution of the Lamb wave propagation, which through inverse FFT produces the time domain signal. As the Lamb modes are generated first, they need to be stored separately. Towards this end, data are collected from the generated modes at several discrete points in the whole range of frequency. Next, a cubic spline interpolation is performed for a very fine frequency step within the same range. While generating the time domain data, interpolation is performed from these finely graded data to get the phase speed (and hence, η).

To get the time history of propagating Lamb waves, a modulated pulse of 200 kHz centre frequency is applied at one end of an infinite plate and X and Z velocities are measured for a propagating distance of 320 h, where h is the thickness of the plate. While studying the time domain representation, the thickness of the plate is taken as 10 mm, which amounts to a frequency-thickness value of *2*. This increased thickness is taken because for this value, at least three modes will be excited in all the cases, as shown by their respective dispersion curves (Figs. 6, 8, 10). To get the same frequency-thickness value otherwise, we have to increase the frequency content of the load to 750 or 800 kHz, which is computationally prohibitive.

In all the plots of Lamb modes, the abscissa is given in terms of frequency times the thickness. Figure 6 shows the first 10 Lamb modes for fibre angle 0°. As is seen in there, first anti-symmetric mode (Mode 1) converges to a value of 1719 m/s in a range of 1 MHz-mm, where all the other modes converge at various later values of frequency. In analogy to the isotropic case, this is the velocity of Rayleigh surface waves in 0° fibre laminae. The first symmetric mode (Mode 2) starts above 10000 m/s and drops suddenly at around 1.3 MHz-mm to converge to 1719 m/s, before which it has fairly constant value. All the other higher order modes escape to infinity at various points in the frequency range. Also the symmetric and anti-symmetric pair of each mode escapes almost at the same frequency.

Propagation of these modes are plotted in Fig. 7 for first three modes ($\boldsymbol{A}_0$, $\boldsymbol{S}_0$, and $\boldsymbol{A}_1$), here referred as Mode 1, 2 and 3 respectively. In left of Fig. 7, the Z velocity history is plotted, whereas in the right of Fig. 7, the X velocity history is plotted. The figures readily show the different propagating modes, each corresponds to one blob. It is to be noted that, wave propagation velocity is given by the group speed (and not the phase speed). Hence, Fig. 6 will not help us to predict the appearances of different modes. However, as Fig. 7 suggest, mode 2 has a lower group speed than mode 1 and mode 3 has a group speed much higher than both mode 1 and 2. One difference in the $\dot{u}$ and $\dot{w}$ history can be observed. For $\dot{u}$, the higher mode generates velocity of comparatively lesser magnitude, whereas, for $\dot{w}$, the magnitude is highest.

Next the fibre angle is changed to 45° and the Lamb modes are plotted in Fig. 8. Here, the

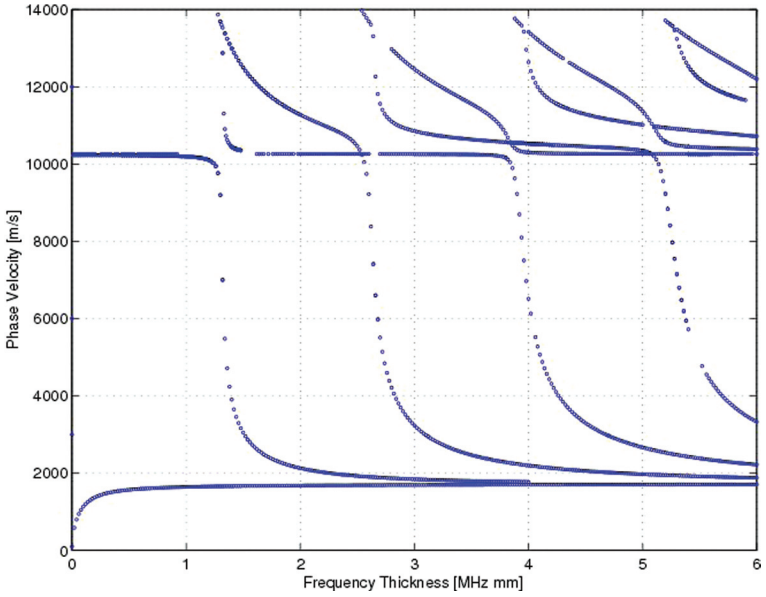

Figure 6: Lamb wave modes for 0° ply angle.

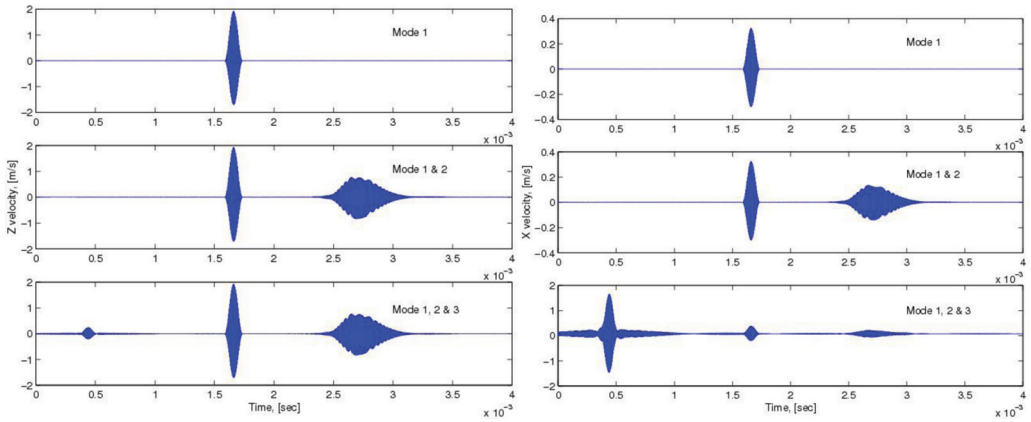

Figure 7: Lamb wave propagation for 0° ply angle laminate for $L = 320\ h$.

phase velocity of Mode 1 (A_0) is lower than the previous values for 0° (1690 m/s). Also, initial phase velocity of Mode 2 (S_0) has come down to less than 6000 m/s in comparison to its 0° counterpart (10000 m/s). Further, the cut-off frequencies of all the higher modes are smaller compared to the previous case. Also there are considerable differences in these cut-off frequencies for each pair of symmetric and anti-symmetric modes, which is absent in the 0° case. Also the number of modes is increased to 11 from 10 in the previous case. The time domain representations of the propagating waves are shown in Fig. 9. In this case, however, the second mode has higher group velocity than the first mode and the third mode has the highest group speed.

Finally, the fibre angle is changed to 90° and the resulting mode shapes are plotted in Fig. 10. The shifting of the modes to the left of the figure continues as the number of modes is increased to 12. Further, the first symmetric mode has come down to 2600 m/s and the first anti-symmetric mode is reduced to a converged speed of 1510 m/s. For these modes the propagating Lamb wave is plotted in Fig. 11 for $\dot{u}$ and $\dot{w}$, respectively. As the figures suggest, mode 2 again has lower group speed compared to mode 1 and mode 3 has higher speed than both mode 1 and 2. However, the difference between the mode 3 group speed and mode

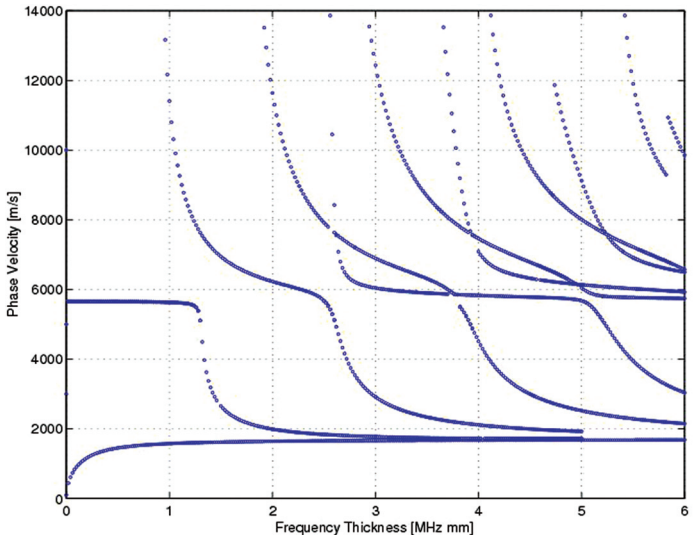

Figure 8: Lamb wave modes for 45° ply angle.

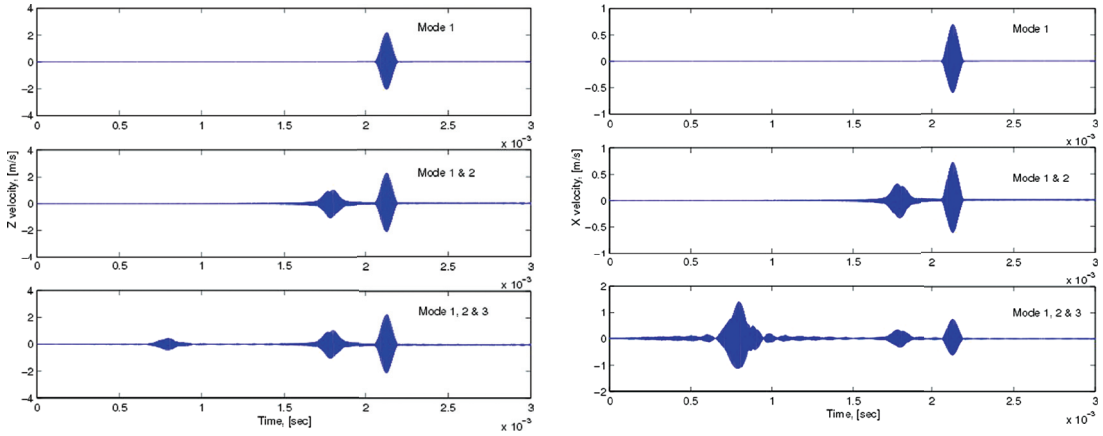

Figure 9: Lamb wave propagation for 45° ply angle laminate for $L = 320\ h$.

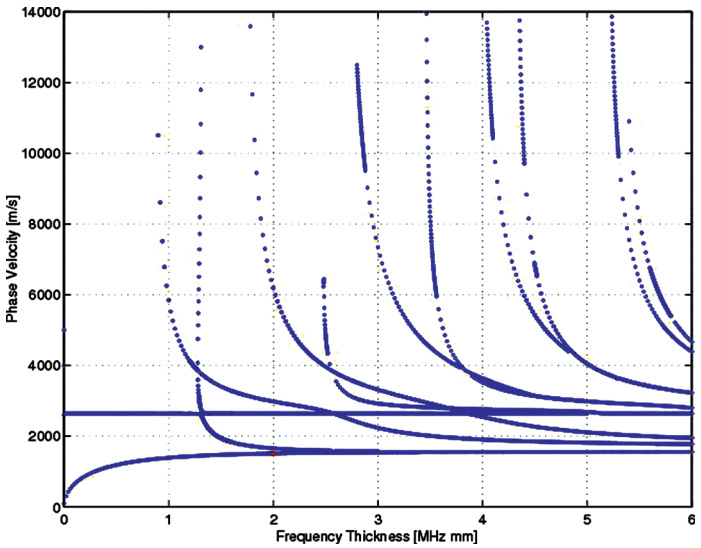

Figure 10: Lamb wave modes for 90° ply angle.

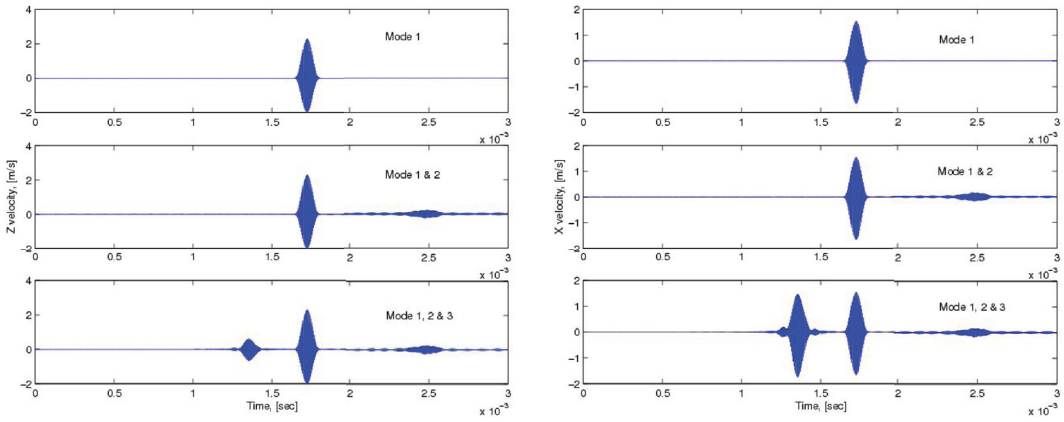

Figure 11: Lamb wave propagation for 90° ply angle laminate for $L = 320\ h$.

2 group speeds is not very high as opposed to the previous cases.

The study of Lamb wave propagation reveals some important effects of ply-angle. It is observed that increase in the ply-angle increases the number of active modes within a defined frequency range, reduces the cut-off frequencies and the phase speeds of a particular mode. Moreover, the difference in the cut-off frequencies increases with the increase in ply-angle.

6 Conclusions

This paper presents an elegant method of determining the Lamb wave modes using spectrally formulated 2-D finite element. First the method of predicting Lamb wave modes for isotropic (metallic) structures is presented using the conventional method of solving the governing Navier's equation. This is done using the method of potentials. This method, however, is not applicable for composites, wherein the method of Partial Wave Technique is used to formulate 2-D spectral finite element, which is then used to solve for Lamb wave modes. This method, does not explicitly involve solution of transcendental equation, which is normally obtained in the case of conventional method of solving for Lamb wave modes. The formulated method is used to obtain Lamb wave dispersion plots in composites for different ply angles and the different propagating Lamb wave modes is shown using time history plots. The develop method is highly suited for automation and can be easily implemented in any software dealing with Structural Health Monitoring.

Acknowledgement

The part of the work reported here is from the thesis of the author's former graduate student Dr. Abir Chakraborty for which the author would like to deeply thank him.

Received 11 September 2013.

References

1. Jones, R.M., Mechanics of Composites Materials, McGraw-Hill Book Company, Washington, D.C., 1975.
2. Sohn, H., Farrar, C.R., Hemez, F.M., Czarnecki, J.J., Shunk, D.D., Stinemates, D.W. and Nadler, B.R. 2003, "A Review of Structural Health Monitoring Literature: 1996–2001". Los Alamos National Laboratory Report, LA-13976-MS.
3. Reid S.R., Zhou G., Impact behaviour of fibre-reinforced composite materials and structures, CRC Press Cambridge, 2000.
4. Gopalakrishnan S., Ruzzene M. and Hanagud S., Computational techniques in Structural Health Monitoring, Springer-Verlag, London, 2011.
5. Lamb H. On waves in an elastic plate. Proc R Soc A—Math Phys Eng Sci 1917;93(648):114–28.
6. Gopalakrishnan S., Chakraborty A. and Roy Mahapatra D., Spectral Finite Element Method, Springer-Verlag, London, 2008.
7. Doyle J.F., Wave Propagation in Structures, Springer-Verlag, New York, 1997.
8. Graff K.F. , Wave Motion in Solids, Dover Publications.
9. Tauchert T.R., Guzelsu A.N. An experimental study of dispersion of stress waves in fiber-reinforced composites. J Appl Mech 1972;35(1):98–102.
10. Nayfeh A.H., Chimenti D.E. Free wave propagation in plates of general anisotropic media. J Appl Mech 1989;56(4):881–6.
11. Nayfeh A.H. The general problem of elastic wave propagation in multi-layered anisotropic media. J Acoust Soc Am 1991;89(4): 1521–31.
12. Yuan F.G., Hsieh C.C. Three-dimensional wave propagation in composite cylindrical shells. Compos Struct 1998;42(2):153–67.

13. Neau G. Lamb waves in anisotropic viscoelastic plates. Study of the wave fronts and attenuation. Ph.D. dissertation. L'Universite de Bordeaux; 2003.
14. Moon F.C. Wave surfaces due to impact on anisotropic plates. J Compos Mater 1972;6:62–79.
15. Whitney J.M., Sun C.T. A higher order theory for extensional motion of laminated composites. J Sound Vibr 1973;30(1):85–97.
16. Lima W.J.N., Braga A.M.B. Dispersive waves in composites, a comparison between various laminated plate theories. Compos Struct 1993;25(1–4):449–57.
17. Liu G.R., Xi Z.C. Elastic waves in anisotropic laminates. Boca Raton (FL): CRC Press; 2002.
18. Rizzi S.A., A spectral analysis approach to wave propagation in layered solids, Ph.D. Thesis, Purdue University, West Lafayette, 1989.
19. Rose J.L., Ultrasonic waves in solid media, Cambridge University Press, 1999.
20. Reddy J.N., Mechanics of Laminated Composite Plates, CRC Press, USA, 1997;117–118.

Dr. Gopalakrishnan is currently a Professor in the department of Aerospace Engineering at Indian Institute of Science. He received his M.Tech degree in Engineering mechanics from IIT, Madras, Chennai and Ph.D degree from the School of Aeronautics and Astronautics, Purdue University, USA. His main areas of interests are, wave propagation in complex medium, structural health monitoring and modelling of nano structures. He is the Associate Editor of *Smart Material and Structures* and *Structural Health Monitoring* Journals and in addition, he is in the editorial boards of 8 other journals. Prof. Gopalakrishnan is an elected Fellow of Indian Academy of Engineering and Indian Academy of Sciences and he is the recipient of Distinguished Alumnus Award from IIT, Madras, Chennai and Distinguished Visiting Fellowship from Royal Academy of Engineering, UK. He has authored 5 graduate level text books, two undergraduate text books, 160 refereed international journal papers, over 100 international conference papers and 8 book chapters.